CHEMISTRY
A European Journal

A Journal of
ChemPubSoc Europe

Accepted Article

Title: Cyclic Bisporphyrin Based Flexible Molecular Containers: Controlling Guest Arrangements and Supramolecular Catalysis by Tuning Cavity Size

Authors: Sankar Prasad Rath, Pritam Mondal, and Sabyasachi Sarkar

To be cited as: *Chem. Eur. J.* 10.1002/chem.201700577

Link to VoR: http://dx.doi.org/10.1002/chem.201700577

Supported by
ACES

WILEY-VCH

10.1002/chem.201700577

WILEY-VCH

Cyclic Bisporphyrin Based Flexible Molecular Containers: Controlling Guest Arrangements and Supramolecular Catalysis by Tuning Cavity Size

Pritam Mondal, Sabyasachi Sarkar and Sankar Prasad Rath*[a]

Abstract: Three cyclic zinc(II) bisporphyrins (**CB**) with highly flexible linkers are employed as artificial molecular containers that efficiently encapsulate/coordinate various aromatic aldehydes within their cavities. Interestingly, the arrangements of the guests and their reactivity inside the molecular clefts are significantly influenced by the cavity size of the cyclic containers. In presence of polycyclic aromatic aldehydes such as 3-formylperylene as a guest, the cyclic bisporphyrin host having smaller cavity (**CB1**) forms 1:1 sandwich complex. Upon slight increase of the spacer length and thereby cavity size, the cyclic host (**CB2**) encapsulates two molecules of 3-formylperylene that are also stacked together due to strong π-π interactions between them and CH-π interactions with the porphyrin rings. However, in the cyclic host (**CB3**) with even large cavity, two metal centers of the bisporphyrin axially coordinate two molecules of 3-formylperylene within its cavity. Different arrangements of guest inside the cyclic bisporphyrin hosts are investigated using UV-vis, ESI-MS and ^{1}H NMR spectroscopy along with X-ray structure determination of the host-guest complexes. Moreover, strong binding of guests within the cyclic bisporphyrin hosts support the robust nature of the host-guest assemblies in solution. Such preferential binding of the bisporphyrinic cavity towards aromatic aldehydes through encapsulation/coordination has been employed successfully to catalyze the Knoevenagel condensation of a series of polycyclic aldehydes with active methylene compounds (such as Meldrum's acid and 1, 3-dimethylbarbituric acid) under ambient conditions. Interestingly, the yields of the condensed products significantly increase upon increasing spacer lengths of the cyclic bisporphyrins, since more substrates can then be encapsulated within the cavity. Such controllable cavity size of the cyclic containers has profound implications for constructing highly functional and modular enzyme mimics.

Introduction

Over the past several decades, supramolecular chemists have given considerable efforts for the design of artificial molecular entities that can behave as container-like systems.[1] The growing interest of such systems is driven in part by their potential applications and prospects in areas as diverse as recognition,[2] catalysis,[3] and transport.[4] The molecular containers generally offer a confined space to encapsulate various guests within their cavities and the shape of the space determines the arrangement of molecules inside.[5] Such molecular entrapment completely isolates the encapsulated molecules from the bulk solution, which eventually influence and facilitate various chemical reactions within the cavities of the containers. Various molecular containers[6] have been previously reported which facilitate unusual chemical reactivity or promoting specific reactions, often with the goal of mimicking enzymatic catalysis.[7] In this regard, the design of molecular container incorporating covalently linked bisporphyrins has enticed a great deal of attention recently, because of the cofacial arrangement through rigid/flexible linkers, which can act as molecular clefts for the binding and activation of a variety of substrates.[8-10] Of particular interest to our group is the design of bisporphyrins appropriate for the applications involving efficient molecular recognition and catalysis.[11] Bisporphyrin cavities of different shapes and sizes can recognize the substrates for various practical applications, while the presence of metal centers would facilitate the scopes further.[12]

In the present investigation, we have employed three tunable dizinc(II) cyclic bisporphyrins[13] (**CB**) varying spacer lengths as flexible molecular containers that are capable of encapsulating aromatic guests to modulate their reactivity and alter the product distributions efficiently. We observe that the cyclic bisporphyrins efficiently accelerate the Knoevenagel condensation of Meldrum's acid (MA)/1,3-dimethylbarbituric acid (DBA) with a series of polycyclic aldehydes which are otherwise less reactive under ambient conditions in the absence of any catalyst. The cyclic bisporphyrins can preferentially encapsulate/coordinate the polycyclic aldehydes inside its cavity according to the spacer length and after the reaction the condensed products are spontaneously released from the bisporphyrinic cavity due to host-guest size discrepancy. Most interestingly, the yields of the condensation products are regulated by the cavity size of the cyclic bisporphyrins, more specifically the spacer length of the bisporphyrins. As the spacer length of the cyclic host increases, the yield of the condensed product also increases. So far, various metal-organic frameworks, zeolites, and covalent organic frameworks are used to act as a size-selective catalyst,[14] which means the selective conversion of one substrate over others based on their size. However, influencing the product distribution by tuning the container's binding pocket is rarely known in literature[15] and detailed understanding will most certainly result in many promising developments and applications in the field of molecular container and catalysis.

[a] P. Mondal, Prof. Dr. S. P. Rath
Department of Chemistry, Indian Institute of Technology Kanpur, Kanpur-208016, India.
E-mail: sprath@iitk.ac.in
Homepage: http://home.iitk.ac.in/~sprath/

Supporting information for this article is given via a link at the end of the document.

Results and Discussion

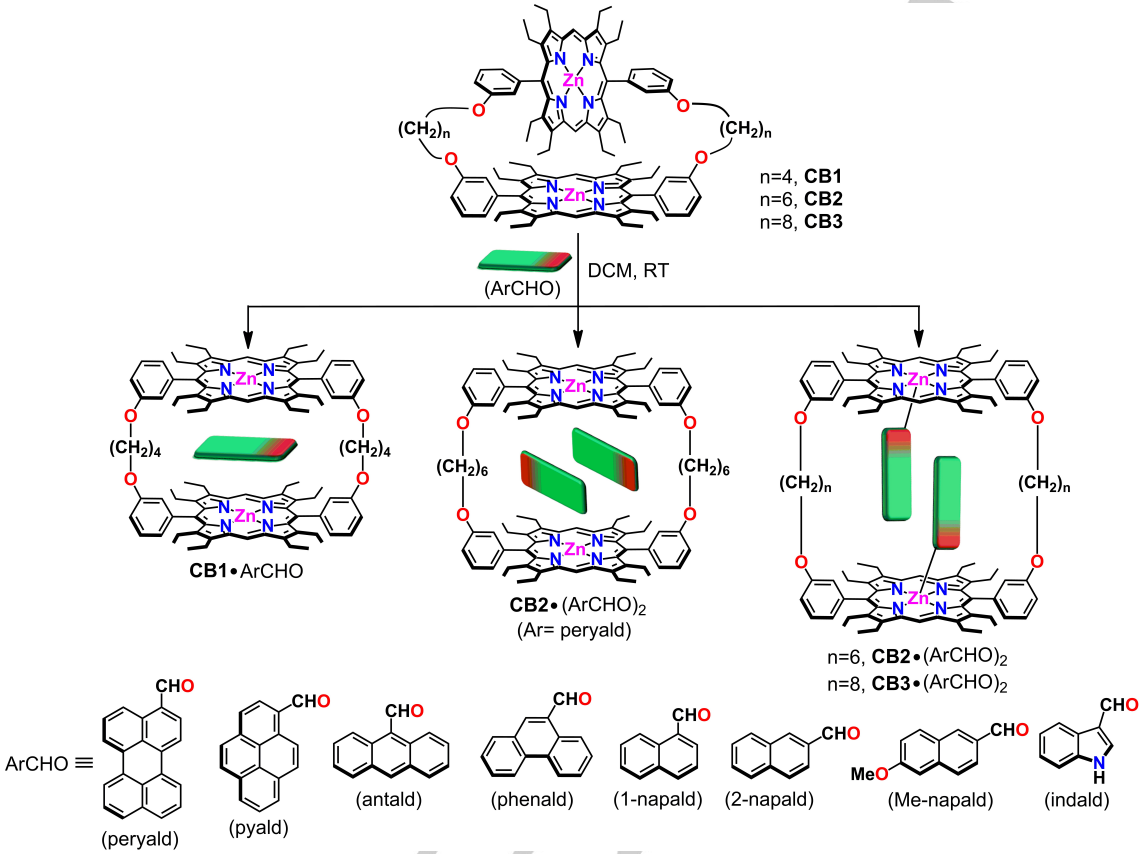

Scheme 1. Cyclic bisporphyrins and their complexes with aldehydes.

Dizinc(II) cyclic bisporphyrin hosts, **CB1** and **CB2** have been prepared using the procedures reported earlier.[13c, d] **CB3** has been synthesized by alkaline-mediated coupling of the corresponding bromoalkylated mono porphyrin with another mono porphyrin having phenol functionalities. Further stirring at room temperature with an excess of zinc acetate in methanol followed by chromatographic purification yielded dark red **CB3** and unambiguously characterized by ^{1}H NMR, ESI-MS, and X-ray crystallography. The synthetic outline is displayed in Scheme S1.

The interactions of the cyclic hosts with polycyclic guests are probed using UV-visible spectroscopy (Figure 1). The absorption spectrum of **CB1** (in dichloromethane) shows an intense Soret band at 409 nm and two Q bands at 541 and 575 nm. Upon incremental addition of 3-formylperylene (peryald) to the dichloromethane solution of **CB1**, the Soret band intensity decreases and slightly red shifted (from 409 to 410 nm) (Figure 1A) due to the formation of the 1:1 sandwich complex which has been isolated in solid as **CB1**·peryald and spectroscopically characterized.

Similarly, upon gradual addition of peryald to a dichloromethane solution of **CB2**, the intensity of the Soret band decreases and red shifted (from 410 to 411 nm) (Figure 1B) owing to the formation of **CB2**·(peryald)$_2$, which has also been isolated and structurally characterized. However, in case of **CB3**, a modest bathochromic shift (410 to 413 nm) with a concomitant decrease in absorption in the Soret band intensity is observed upon addition of peryald. During such transformation, several isosbestic points are also observed at 386, 421, 515, 590 nm (Figure 1C) and the corresponding host-guest complex is isolated and structurally characterized as **CB3**·(peryald)$_2$. Similarly, the interactions of the cyclic bisporphyrins (**CB**) with other aromatic aldehydes, *e.g.* pyrene-1-carbaldehyde (pyald) and 9-anthraldehyde (antald) are also monitored using UV-visible spectroscopy and displayed in Figures S1-S2. Scheme 1 portrays the synthetic outline of all the complexes along with the abbreviations used.

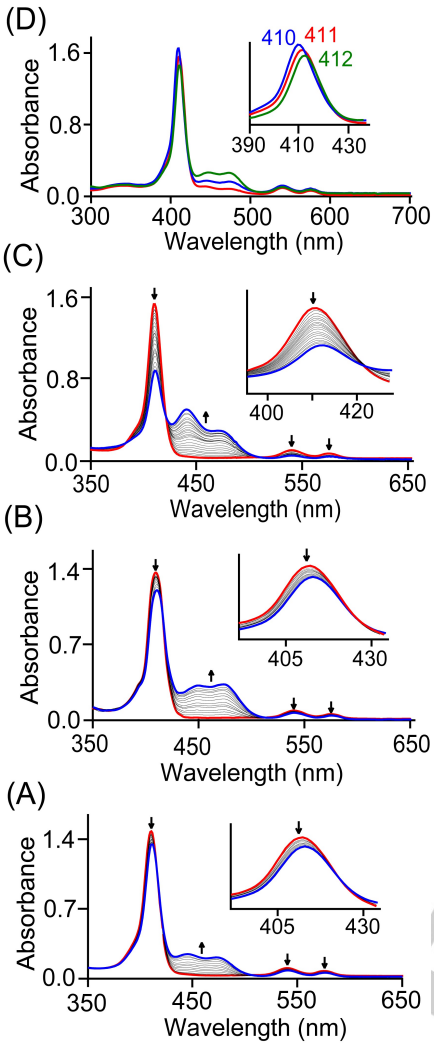

Figure 1. UV-visible spectral changes (at 298K in dichloromethane) of (A) **CB1** (3×10^{-6} M) upon addition of peryald as the **CB1**:peryald molar ratio changes from 1:0 to 1:30, (B) **CB2** (3×10^{-6} M) upon addition of peryald as the **CB2**:peryald molar ratio changes from 1:0 to 1:65, (C) **CB3** (3×10^{-6} M) upon addition of peryald as the **CB3**:peryald molar ratio changes from 1:0 to 1:80, and (D) UV-visible spectra of polycrystalline samples of **CB1**·peryald (red), **CB2**·$(peryald)_2$ (blue), **CB3**·$(peryald)_2$ (green). Arrows indicate the increasing or decreasing trend in intensity.

The formation of the host-guest complexes are further substantiated by ESI-MS spectroscopy. ESI mass spectra of polycrystalline sample of **CB1**·peryald reveals the desired signal at m/z 1953.8616, which is assigned to [**CB1**·peryald+H]$^+$ (Figure S3), and thus confirms the formation of 1:1 inclusion complex between the host (**CB1**) and the guest (peryald). However, in case of **CB2**·$(peryald)_2$ and **CB3**·$(peryald)_2$, the desired signals at 1144.3190 and 2344.1565 are observed for [**CB2**·$(peryald)_2$+2H]$^{2+}$ and [**CB3**·$(peryald)_2$+H]$^+$, respectively, which manifest the formation of 1:2 complexes between the hosts (**CB2** and **CB3**) and the guest (peryald) (Figure S4). Moreover, the experimental peaks are isotopically resolved and are also in good agreement with their theoretical distributions.

X-ray structures of the host-guest complexes **CB2**·$(peryald)_2$ and **CB3**·$(peryald)_2$ are reported here, which allow us to make a direct structural and spectroscopic comparison upon guest binding. Although the single crystals of **CB1**·peryald, suitable for X- ray structure determination, could not be obtained, but the complex is geometrically optimized using density functional theory (DFT) (*vide infra*). Additionally, X-ray structures of the host-guest complexes between **CB1** and 6-methoxy 2-naphthaldehyde (**CB1**·Me-napald), **CB2** and 9-anthraldehyde [**CB2**·$(antald)_2$], **CB3** and pyrene-1-carbaldehyde [**CB3**·$(pyald)_2$] are also reported here, which further offer substantial insight into the rational control over guest encapsulation and also the reactivity therein. Detailed synthetic procedures of all the host-guest complexes and their spectral characterizations are provided in the experimental section.

Crystallographic characterization

Dark red crystals of **CB1**·Me-napald are obtained through slow diffusion of *n*-hexane into a solution of the respective complex in dichloromethane. The complex crystallizes in the monoclinic crystal system with *C*2/c space group. Perspective view of **CB1**·Me-napald is displayed in Figure 2, while the molecular packing is shown in Figure S5. In **CB1**·Me-napald, the Zn centers have four-coordinate square-planar geometry and the average Zn–N_{por} distance is 2.04 Å, which is a typical distance observed in the X-ray structure of Zn(II) porphyrins known in the literature.[9a, f] The intramolecular Zn···Zn nonbonding distance is found to be 6.31 Å, while the C_{meso}···C_{meso} distance is 7.047 Å.

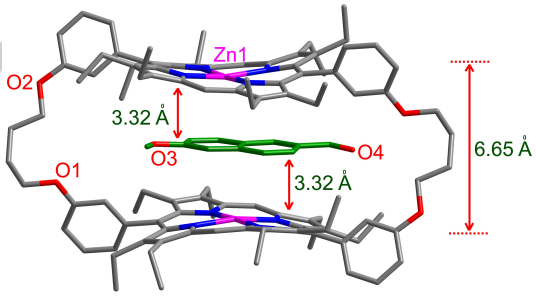

Figure 2. A perspective view of X-ray crystal structure (at 100 K) of **CB1**·Me-napald (H atoms and solvent molecules have been omitted for clarity). Distances shown are the separation between two mean planes.

As can be seen in the structure, a Me-napald molecule is sandwiched between the two porphyrin rings with an average Me-napald···porphyrin distance of ~3.32 Å. Moreover, the guest (Me-napald) and porphyrin rings are also nearly coplanar, with a small offset that manifests strong π-π interactions to form a robust host–guest assembly.

The dark-red crystals of **CB2**·$(peryald)_2$ are grown *via* slow diffusion of acetonitrile into the dichloromethane solution of the compound. The compound crystallizes in the triclinic crystal system with *P*-1 space group. Perspective view of **CB2**·$(peryald)_2$ is displayed in Figure 3A, while the molecular packing is depicted in Figure S6. In **CB2**·$(peryald)_2$, two Zn centers have four-coordinate square-planar geometry with the

metal center close to the least squares plane of the $C_{20}N_4$ porphyrinato core. The average Zn–N_{por} and the intramolecular Zn···Zn nonbonding distance is found to be 2.039 Å and 11.50 Å, respectively, whereas, the C_{meso}···C_{meso} distance is 11.67 Å. As can be seen in the structure, two peryald molecules are cofacially stacked together in the bisporphyrinic cleft with an angle of 60.10° with the $C_{20}N_4$ porphyrinato plane. The average distance between two encapsulated peryald molecules is 3.40 Å, which shows an appreciable π-π interaction between them (Figure 3B). Also, the average distance from the nearest peryald carbon atom to $C_{20}N_4$ porphyrinato plane is found to be 3.32 Å, leading to a strong CH-π interaction with the porphyrin ring (Figure S7) which eventually facilitates the unusual stacking of the guests that are observed.

Dark-red crystals of **CB2**·(antald)$_2$ are obtained similarly as described above and the complex crystallizes in the monoclinic crystal system with $P2_1/n$ space group. Perspective view of **CB2**·(antald)$_2$ is displayed in Figure 3C and Figure S8 illustrates the molecular packing. In **CB2**·(antald)$_2$, each Zn center has five-coordinate square-pyramidal geometry in which the metal centers are displaced by approximately 0.28 Å from the mean porphyrin plane. The average Zn-N_{por} and intramolecular Zn···Zn nonbonding separation are found to be 2.060 and 11.077 Å.

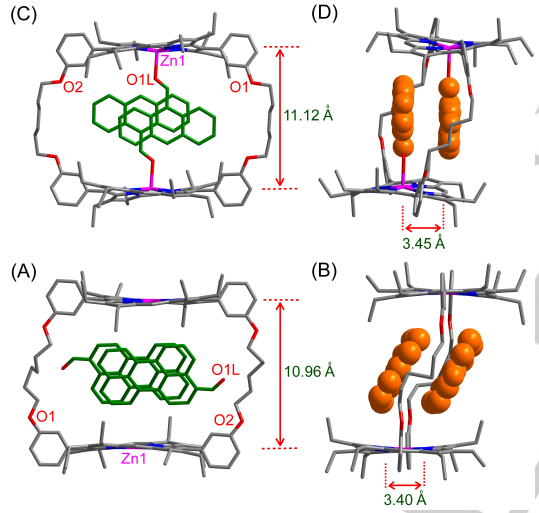

Figure 3. (A) Perspective view of X-ray crystal structure (at 100 K) of **CB2**·(peryald)$_2$, (B) diagram illustrating the interactions between two peryald molecules inside **CB2**, (C) perspective view of X-ray crystal structure (at 100 K) of **CB2**·(antald)$_2$, and (D) diagram illustrating the interactions between two antald molecules inside **CB2** (H atoms and solvent molecules have been omitted for clarity). Distances shown are the separation between two mean planes.

As can be seen in the crystal structure, two antald molecules are axially coordinated to the Zn centers of the porphyrin units with the aldehyde 'O' atom (Zn–O_{ax}: 2.153 Å), and the intermolecular separation between two cofacially stacked antald molecules inside the cleft is 3.45 Å (Figure 3D). Due to the smaller size of the antald (7.29 Å×4.25 Å), **CB2** can easily accomodate and axially coordinates within its cavity to form **CB2**·(antald)$_2$, whereas, peryald, having lager size (9.84×4.85 Å) could not coordinate with the Zn atoms and stacked unusually inside the **CB2** cavity in **CB2**·(peryald)$_2$. The selected bond distances and angles are listed in Table 1, while crystal data and data collection parameters are given in Table S1.

The dark red crystals of **CB3**·(peryald)$_2$ and **CB3**·(pyald)$_2$ are grown *via* slow diffusion of *n*-hexane into the dichloromethane solutions of the respective complexes and both the complexes crystallize in the triclinic crystal system with *P*-1 space group. Perspective views of **CB3**·(peryald)$_2$ and **CB3**·(pyald)$_2$ are displayed in Figure 4. In both the complexes, each Zn centre has five-coordinate square-pyramidal geometry in which the metal ions are displaced by approximately 0.25 Å [**CB3**·(peryald)$_2$] and 0.33 Å [**CB3**·(pyald)$_2$] from the $C_{20}N_4$ porphyrinato core. The Zn–N_{por} distances are found to be 2.051 and 2.075 Å, whereas, Zn-O_{ax} distances are 2.196 and 2.189 Å for **CB3**·(peryald)$_2$ and **CB3**·(pyald)$_2$, respectively. The intramolecular Zn···Zn nonbonding distances are found to be 15.493 Å [**CB3**·(peryald)$_2$] and 13.069 Å [**CB3**·(pyald)$_2$].

As can be seen from the structure of **CB3**·(peryald)$_2$, the two peryald molecules are axially coordinated to two Zn centers of the **CB3** with the aldehyde 'O' atom, as also observed in the case of **CB2**·(antald)$_2$ and the separation between two cofacially stacked peryald guests inside the cleft is 3.33 Å (Figure 4B). Such axial coordination of peryald is possible due to the larger cavity size of **CB3**, which is not attainable with **CB1** and **CB2**. However, two more peryald guests are stacked between two molecules of **CB3**·(peryald)$_2$ with an average distance of 3.43 Å between them. The average non bonding separation between the coordinated

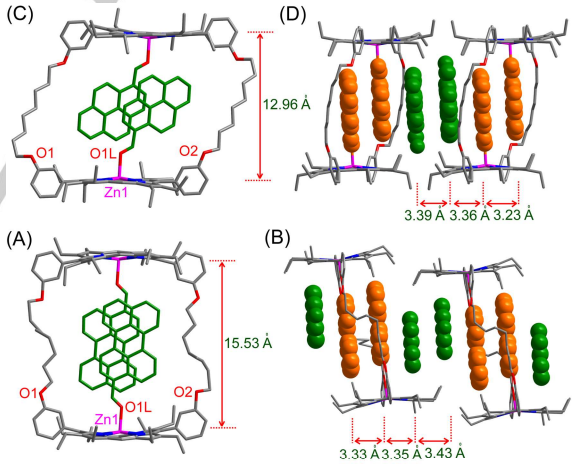

Figure 4. (A) Perspective view of X-ray crystal structure (at 100 K) of **CB3**·(peryald)$_2$, (B) diagram illustrating the interactions between peryald molecules inside **CB3**, (C) perspective view of X- ray crystal structure (at 100 K) of **CB3**·(pyald)$_2$, and (D) diagram illustrating the interactions between pyald molecules inside **CB3** (H atoms and solvent molecules have been omitted for clarity). Distances shown are the separation between two mean planes.

and the non-coordinated peryald molecules are found to be 3.35 Å and thus form strong π-π interaction between them. Furthermore, the stacking arrangement of the non-coordinated peryald molecules are stabilized by strong CH-π interactions with the nearby porphyrin ring, as also observed in **CB2**·(peryald)$_2$. Similar stacking pattern is also observed in case of **CB3**·(pyald)$_2$, where the interplanar distance between

Table 1. Selected bond lengths (Å) and bond angles (°).

Bond lengths, (Å)	**CB1**·Me-napald	**CB2**·(peryald)$_2$	**CB2**·(antald)$_2$	**CB3**·(peryald)$_2$	**CB3**·(pyald)$_2$
Zn(1)-N(1)	2.041(5)	2.039(2)	2.063(2)	2.034(6)	2.086(5)
Zn(1)-N(2)	2.039(5)	2.043(2)	2.061(2)	2.050(6)	2.073(6)
Zn(1)-N(3)	2.040(6)	2.036(2)	2.052(2)	2.061(6)	2.060(6)
Zn(1)-N(4)	2.040(5)	2.039(2)	2.067(2)	2.061(6)	2.083(6)
Zn(1)-O(1L)	-	-	2.153(2)	2.196(5)	2.189(5)
Bond angles, (°)					
N(1)- Zn(1)-N(2)	92.4(2)	92.71(9)	92.26(9)	92.6(2)	91.6(2)
N(1)- Zn(1)-N(3)	176.6(2)	179.31(9)	170.34(9)	168.1(2)	165.8(2)
N(1)- Zn(1)-N(4)	87.0(2)	87.10(9)	86.04(9)	86.2(2)	85.7(2)
N(2)- Zn(1)-N(3)	87.3(2)	87.51(9)	86.72(9)	86.3(2)	86.9(2)
N(2)- Zn(1)-N(4)	170.4(2)	176.50(10)	162.83(9)	167.8(2)	165.6(2)
N(3)- Zn(1)-N(4)	92.7(2)	92.71(9)	92.10(9)	92.3(2)	92.3(2)
N(1)-Zn(1)-O(1L)	-	-	97.16(8)	100.1(2)	97.4(2)
N(2)-Zn(1)-O(1L)	-	-	95.94(8)	93.6(2)	100.2(2)
N(3)-Zn(1)-O(1L)	-	-	92.50(8)	91.7(2)	96.7(2)
N(4)-Zn(1)-O(1L)	-	-	101.22(8)	98.6(2)	94.2(2)

coordinated pyald molecules is 3.29 Å and the non-coordinated pyald molecules is 3.39 Å (Figure 4D). Figures S9 and S10 depict the molecular packing of **CB3**·(peryald)$_2$ and **CB3**·(pyald)$_2$, respectively, whereas, the selected bond distances and angles are provided in Table 1.

The salient structural features of all the complexes, reported herein, are compared in Table 2 which further enable us to analyze the structural and conformational changes upon guest entrapment within the bisporphyrin hosts. X-ray structure of **CB2** has been reported by us previously[9a], where two porphyrin rings are aligned in a perpendicular fashion to each other with an angle of 84.97°. However, upon intercalation of two peryald molecules, the two perpendicular rings immediately switches to parallel orientation with a zero interplanar angle in **CB2**·(peryald)$_2$. Similar observations are also obtained for other complexes reported here. Axial coordination has increased Zn-N_{por} distance and metal displacement from the mean porphyrin plane (Δ^{Zn}_{24}). The average mean plane separation is found to be highest in case of **CB3**·(peryald)$_2$ (15.53 Å), while, lowest in case of **CB1**·Me-napald (6.65 Å). Similarly, the intramolecular Zn···Zn and C_{meso}···C_{meso} nonbonding distances are also found to be maximum in case of **CB3**·(peryald)$_2$, which are 15.493 Å and 15.384 Å, respectively, whereas, lowest in case of **CB1**·Me-napald. Also, due to axial coordination, the displacement (in Å) of metal atom from the $C_{20}N_4$ porphyrinato core is higher in case of **CB2**·(antald)$_2$, **CB3**·(peryald)$_2$, and **CB3**·(pyald)$_2$ than the other three complexes *viz*. **CB2**, **CB1**·Me-napald, and **CB2**·(peryald)$_2$. Thus, the comparative structural analyses between the complexes clearly manifest the exceptional ability of the cyclic bisporphyrin platforms to flip its cavity by a large vertical displacement. Such a unique feature is due to the presence of flexible linkers that can easily be folded to adjust the various conformations according to the shape and size of the guests.

Table 2. Selected structural parameters of the complexes.

Complex	Zn-N_{por}[a]	Δ^{Zn}_{24}[b]	Δ_{24}[c]	MPS[d]	C_m···C_m[e]	Zn···Zn[a]	θ[f]	Ref
CB2	2.035	0.09	0.18	-	9.114	9.018	84.97	9a
CB1·Me-napald	2.040	0.18	0.26	6.65	7.047	6.312	0.00	tw
CB2·(peryald)$_2$	2.039	0.03	0.14	10.96	11.672	11.500	0.00	tw
CB2·(antald)$_2$	2.060	0.28	0.24	11.13	11.440	11.077	0.00	tw
CB3·(peryald)$_2$	2.051	0.25	0.19	15.53	15.384	15.493	0.00	tw
CB3·(pyald)$_2$	2.075	0.33	0.08	12.96	13.644	13.069	0.00	tw

[a] Average value in Å. [b] Displacement (in Å) of Zn from the least-square plane of $C_{20}N_4$ porphyrinato core. [c] Average displacement (in Å) of atoms from the least-square plane of $C_{20}N_4$ porphyrinato core. [d] Average distance (in Å) of two least-squares plane of $C_{20}N_4$ porphyrinato core. [e] Non-bonding distance (in Å) between two *meso* carbons that are covalently connected. [f] Angle between two least-square planes of $C_{20}N_4$ porphyrinato core

NMR spectroscopy

^{1}H NMR titration experiments are performed at 298 K in $CDCl_3$ to gain further insight into the host–guest complexation process in solution. Usually, cyclic bisporphyrins, **CB** exist in solution as a mixture of conformational isomers due to its flexible linkers, thus showing a complicated ^{1}H NMR spectrum.[11b] However, upon addition of guest ligands, the spectra are substantially simplified, indicating that the encapsulation of the guest is accompanied by an induced-fit conformational change in the host molecules. Upon addition of 1 equivalent of peryald to a $CDCl_3$ solution of **CB1,** upfield shift of the guest protons are observed because of close proximity and strong ring current effect of two porphyrin units (trace C, Figure S11). Also, no peaks are observed in the free guest ligand region, which manifest the robust nature of the host-guest assemblies in solution. However, addition of one more equivalent of peryald, no further shifting of the peryald protons are observed (trace D, Figure S11). Figure 5 shows the relevant spectra obtained upon gradual addition of peryald to a

$CDCl_3$ solution of **CB2**. Traces A and B show the spectra of **CB2** and peryald alone, respectively, whereas, traces C and D illustrate the spectra after additions of one and two equivalents of peryald, respectively. As can be seen from the spectra, the largest upfield shifts of the peryald protons take place when two equivalents of peryald are added. Even after the addition of more than two equivalents of peryald, no further shifting of the peryald protons are observed, which confirms the 1:2 complexation between **CB2** and peryald (trace E, Figure 5)

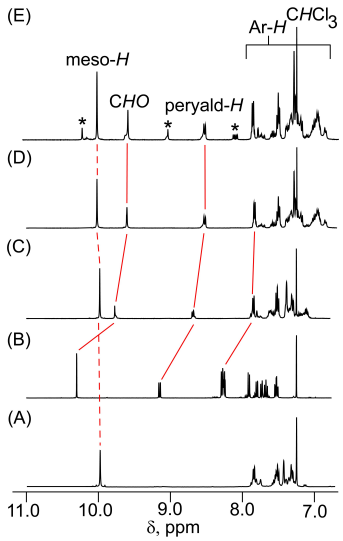

Figure 5. Partial ^{1}H NMR spectra (in $CDCl_3$ at 298 K) of (A) **CB2**, (B) peryald, (C) after addition of 1 eqv. of peryald, (D) after addition of 2 eqv. of peryald, and (E) after addition of 3 eqv. of peryald. Asterisked signals originate from the excess peryald.

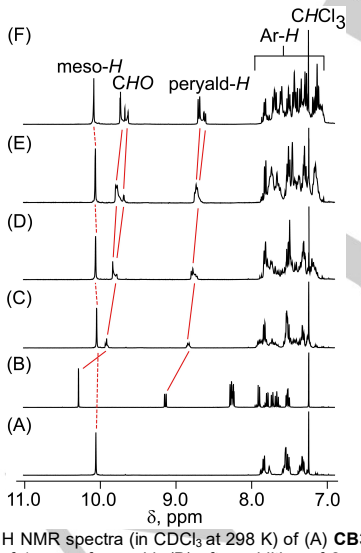

Figure 6. Partial ^{1}H NMR spectra (in $CDCl_3$ at 298 K) of (A) **CB3**, (B) peryald, (C) after addition of 1 eqv. of peryald, (D) after addition of 2 eqv. of peryald, (E) after addition of 3 eqv. of peryald, and (F) after addition of 4 eqv. of peryald.

in solution. A similar observation is obtained upon gradual addition of peryald upto two equivalents into the $CDCl_3$ solution of **CB3** (Figure 6). However, addition of one more equivalent of peryald to **CB3**, another set of peak is generated in the upfield region (trace E, Figure 6). The newly generated peaks are shifted further upfield region upon addition of another equivalent of peryald (trace F, Figure 6). Such shifting of the peryald protons clearly suggests the presence of two different types of peryald in the **CB3**·$(peryald)_2$ assembly, as also observed in the X-ray crystal structure of the complex (*vide supra*). In sharp contrast, slight upfield shifts of the peryald protons are observed when monomeric unit of the cyclic host [5,15-bis(3′-hydroxyphenyl)-octaethylporphyrin, mono] is used in the titration, as shown in Figure S12.

Association constant determination

The association constants for all the host-guest complexes are determined by the UV-visible spectroscopic titration method, which clearly rationalize the efficient binding and stoichiometry of the host-guest complexes. The association constants are calculated using the HypSpec computer program (Protonic Software, U.K.), while the species distribution plots of the complexes are calculated using the program HySS2009 (Protonic Software, U.K.).[16] During the experiment, the concentrations of the cyclic hosts **CB** are kept constant at 3×10^{-6} M while the concentration of peryald is varied within the range of 10^{-6}-10^{-4} M. The association constants between the host and guest are calculated by measuring the changes in intensity of the peak at 450 nm in the UV-visible spectra. Best-fits are obtained for the 1:1 binding between the **CB1** and peryald with an association constant of $6.3\pm0.2\times10^5$ M^{-1}. However, best-fits are obtained by applying two step binding model, 1:1 (K_1) and 1:2 (K_2) complex, between the hosts (**CB2** and **CB3**) and peryald as guest. For the complexation of peryald, the K_1 and K_2 are found to be $1.3\pm0.2\times10^4$ M^{-1} and $3.8\pm0.3\times10^4$ M^{-1}, respectively, with **CB2** and $1.6\pm0.3\times10^4$ M^{-1} and $2.5\pm0.3\times10^5$ M^{-1}, with **CB3**. Larger value of K_2 suggests the cooperative binding of the guest ligand in the 1:2 host-guest complexes. Figures S13-S15 depict the relevant plots for the binding of peryald within the cyclic bisporphyrin hosts.

CB catalyzed Knoevenagel condensation reactions

Generally, in the biological systems, the reactivity of a substrate is tuned by isolating it from the bulk to achieve high selectivity and catalytic activity.[7b,e] In the present investigation, the efficient binding between the polycyclic aromatic aldehyde guests and the cyclic hosts (**CB**) prompted us to investigate the potential application of **CB** as a catalyst for Knoevenagel condensation. Initially, the inclusion complex **CB2**·$(peryald)_2$ is treated with Meldrum's acid (MA, 4 eqv.) in an aqueous THF (1:1) medium at room temperature. After 3 hours of stirring at room temperature, the solution turns dark red and turbid owing to the precipitation of the condensed product (peryald·MA) as a yellowish powder, which is further isolated and characterized by NMR and ESI-MS spectroscopy. ^{1}H NMR spectra show the formation of the condensation product peryald·MA in 50% yield (Figure 7). Without the cyclic host as catalyst, peryald gives only

a trace amount of the condensation product (~3%) under similar experimental condition. ^{1}H NMR spectral measurements also confirm that the condensation product peryald·MA is not properly fitted within **CB2** cavity (Figure S16), since the guest size is too large to be accommodated inside the cavity. The spontaneous release of the condensed product from the bisporphyrinic cavity encourage us to explore further the catalytic efficiency of **CB2** for Knoevenagel condensation of a number of polycyclic aromatic aldehydes with Meldrum's acid (MA) and 1,3-dimethylbarbituric acid (DBA) under ambient conditions. Scheme 2 portrays the synthetic outline of the Knoevenagel condensation of aromatic aldehydes reported here, whereas, detailed synthetic procedure and spectroscopic characterizations of all the condensed products are given in the supporting information (Figures S17-S32).

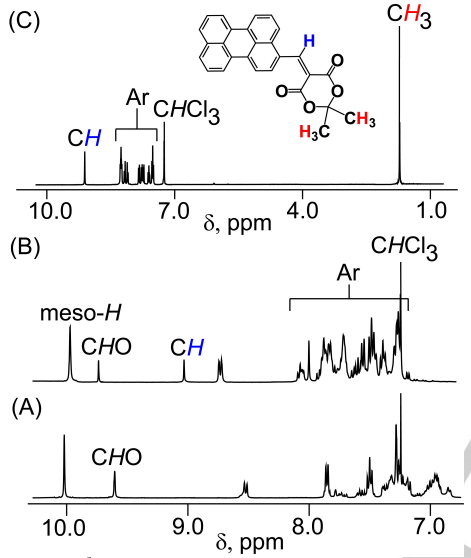

Figure 7. Partial ^{1}H NMR spectra (in $CDCl_3$ at 298 K) of (A) **CB2**·(peryald)$_2$, (B) after the condensation of peryald with MA, (C) condensation product peryald·MA obtained after extraction and purification

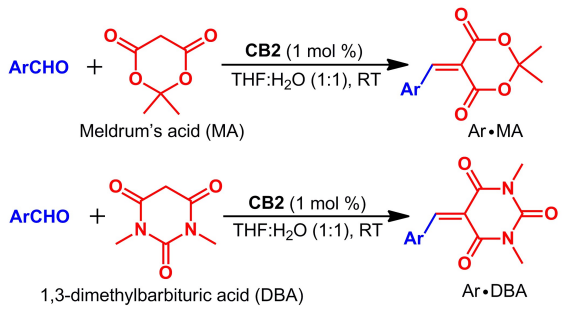

Scheme 2. Knoevenagel condensation of aromatic aldehydes in aqueous THF.

In presence of **CB2** (1 mol %), the condensation between peryald and MA significantly increases to 42% yield within 10 h (with respect to aldehyde). Similarly, the condensation of pyald with MA efficiently promote to 50% within 10 h, whereas, the reaction proceed hardly without **CB2**, 6% (entry 2, Table 3). Moreover, the condensation of sterically hindered antald with MA is efficiently elevated to 35% yield, while the condensation of antald scarcely occur (<2%) without **CB2** (entry 3, Table 3). Similarly, 1-naphthaldehyde gives 1-napald·MA in 48% with **CB2**, whereas, the yield is found to be 12% in the absence of **CB2** (entry 5). In case of other polycyclic aldehydes (*i.e.*, phenald, 2-napald, Me-napald, indald), the condensation reactions are also found much faster in the presence of **CB2**, which, however, proceed poorly with very low yield without **CB2** (Table 3). Similarly, in presence of more-reactive DBA, the yield of the condensation products of all polycyclic aldehydes are significantly increased, which is tabulated in Table S2. In contrast, smaller aldehyde, such as benzaldehyde, which poorly fits into the bisporphyrinic cavity, gives almost similar yield of the

Table 3. Yields of the Knoevenagel condensations of aromatic aldehydes and Meldrum's acid. [a]

Entry	Aldehyde	Reaction time, h	Yield of product, Ar·MA (%)	
			Without **CB2**	With **CB2**
1	peryald	10	3	42
2	pyald	10	6	50
3	antald	72	2	35
4	phenald	10	8	55
5	1-napald	24	12	48
6	2-napald	10	15	72
7	Me-napald	10	16	75
8	indald	10	8	54
9	Benzaldehdye	10	35	40

[a] Reaction conditions: aldehyde (0.10 mmol), MA (0.10 mmol), and bisporphyrin (**CB2**) (1 mol %) in THF:H_2O (5.0 mL) at room temperature. Yields were determined by ^{1}H NMR analysis.

condensed product with MA (35%) corresponding to the reaction without **CB2** (40%) (entry 9, Table 3). Further, we have investigated the condensation reaction of aliphatic aldehyde like cyclohexanecarboxaldehyde and isobutyraldehyde with MA for 10 h in presence of **CB2**, however, no significant enhancement of the yield is observed. Such observation clearly manifests the selectivity of the bisporphyrinic cavity towards the polycyclic aldehydes, which are otherwise less reactive under ambient conditions without any catalyst.

Encouraged by these results, we have further investigated the catalytic activity of the other cyclic hosts (**CB1** and **CB3**) towards the Knoevenagel condensation reaction. Interestingly, we notice that under identical condition, the yields of the condensation products are varied according to the cavity size of the bisporphyrins, more specifically the spacer length of the bisporphyrins. In case of cyclic host with smallest cavity size, **CB1**, the product peryald·MA is obtained in only 17% yield. However, using **CB2**, an impressive progress of the condensation reaction is observed and the product peryald·MA is obtained in 42% yield. Further increasing the cavity size in **CB3**, yield of the product increases significantly upto 50%. Similar observation has also been obtained in case of the condensation reaction of other aldehydes (*i.e.*, pyald, antald and 2-napald) with MA (Table 4). Such observation can be explained in the light of the guest arrangement inside the bisporphyrinic cavity. The sequestering of the aldehydes from the bulk and strong substrate binding within the bisporphyrinic cavity is possibly the primary reason for enhancing the catalytic ability of the **CB**. In case of **CB1**, only one molecule of aldehyde gets encapsulated within the cleft which drives the reaction to the condensed product resulting only a slight increase of the yields.

In case of **CB2**·(peryald)$_2$, however, two aldehyde molecules are held together with a strong π-π stacking interactions which are further stabilized by the CH-π interactions with the porphyrin rings. After the reaction, the condensed products become too bulky for enclathration and readily come out of the cleft and thus easily replaced by the incoming reactants, which eventually increases the yield of the products. However, in case of **CB3**·(peryald)$_2$, the Zn(II) centers of the bisporphyrin coordinatively interacts with the aldehydic 'O' atom to selectively accommodate them inside the macrocyclic cavity and activate the substrates leading to better yield. The accommodations of other aldehydes (such as pyald, antald and 2-napald) inside **CB2** and **CB3** cleft are very similar, although the yields of the condensed products are slightly higher with **CB3**. This is because more number of aldehyde substrates can then be encapsulated in **CB3** due to larger cavity size, as observed in the X-ray crystal structure of the host-guest complexes. Moreover, to justify the cavity effect, a control experiment is performed in presence of monomeric unit of the cyclic host [5,15-bis(3′-hydroxyphenyl)-octaethylporphyrin, mono] which, however, does not regulate the yield of the condensed products (Table 4). Furthermore, the condensation reaction between peryald and MA is performed in different solvent medium, and found that the reaction is significantly promoted in aqueous THF (1:1) medium in a homogeneous fashion. The low solubility of MA in organic solvents (such as chloroform and dichloromethane), and insolubility of **CB** in polar protic solvents (such as methanol, ethanol and water) are responsible for the poor catalytic transformation (Table S3). To check the reusability of the cyclic host, it is separated and collected from the reaction mixture by simple column chromatography. No significant changes have been observed in the isolated cyclic host (Figure S33) and can be easily employed for further catalytic processes.

Table 4. Yields of the products in presence of **CB**.[a]

Entry	Aldehyde	Yield of product, Ar·MA (%)			
		CB1	**CB2**	**CB3**	mono
1	peryald	17	42	50	6
2	pyald	22	50	61	8
3	antald	11	35	42	2
4	2-napald	30	72	82	15

[a] Reaction conditions: aldehyde (0.10 mmol), active methylene compound (0.10 mmol), and bisporphyrin (1 mol %) in THF:H_2O (5.0 mL) at room temperature. Yields are determined by ^{1}H NMR analysis. Reaction time: 10 h (in case of antald, 72 h).

The proposed mechanism for the catalytic Knoevenagel condensation within cyclic host **CB3** is displayed in Figure 8. Generally, water soluble MA is not a suitable guest for **CB3**, and it exists in equilibrium with its enolate form because of its low pKa value.[5a] We assume that, after accommodating the aldehyde inside the bisporphyrin cleft, the enolate form of MA attacks the encapsulated aldehyde. After that, the loss of water readily takes place (due to the hydrophobicity of the cavity) to generate the dehydrated product peryald·MA. Since, the product peryald·MA is too bulky to be fitted within the cavity, it spontaneously comes out of the bisporphyrin cavity while a new aldehyde substrate comes in.

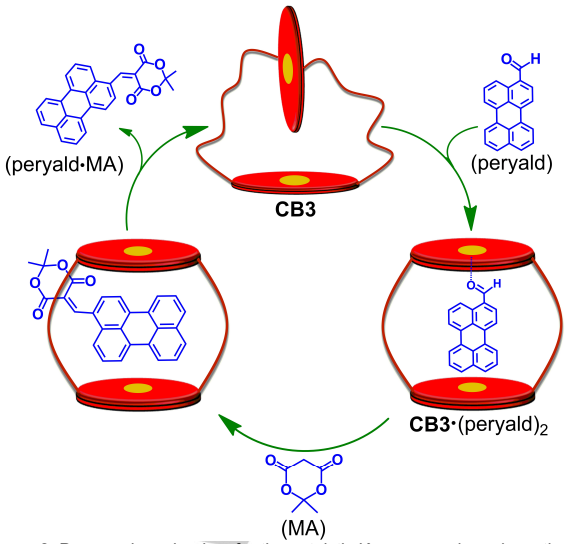

Figure 8. Proposed mechanism for the catalytic Knoevenagel condensation of peryald with MA in the presence of cyclic host **CB3**. For simplicity, only one guest molecule is shown in this catalytic cycle.

Theoretical calculation

Computational studies are carried out by using density functional method (DFT) at the B3LYP/6-31G** level[17] to get further insight of the host-guest assemblies. All the coordinates are taken directly from the X-ray crystal structure of the complexes and all

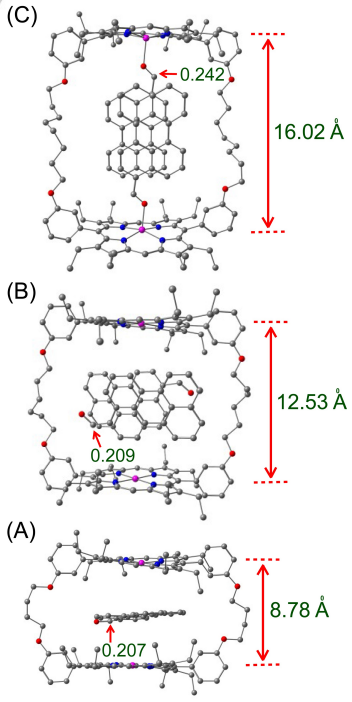

Figure 9. Optimized molecular structure of (A) **CB1**·peryald, (B) **CB2**·(peryald)$_2$, and (C) **CB3**·(peryald)$_2$ calculated by DFT method at the B3LYP/6-31G** level. Values show the Mulliken charges on the formyl carbon of peryald and mean plane separation between two porphyrin rings.

the molecules are successfully optimized. The DFT optimized structures of **CB1**·peryald is displayed in Figure 9 along with the optimized structures of **CB2**·(peryald)$_2$ and **CB3**·(peryald)$_2$, whereas the optimized structure of **CB1**·pyald is displayed in Figure S34. The computed bond distances and angles of **CB1**·peryald and **CB1**·pyald are shown in Table S4. The Mulliken charge density on the formyl carbon atom of the encapsulated aldehydes within **CB** cleft are also calculated and displayed in Figure 9. Due to the axial coordination, the +ve charge on the formyl carbon is highest in case of **CB3**·(peryald)$_2$, resulting a feasible nucleophilic attack of the enolate form of MA. Moreover, we have optimized the geometry of **CB2**·(peryald)$_2$ by stacking the two peryald molecule parallel with the porphyrin planes. However, the original geometry of **CB2**·(peryald)$_2$ is found to be energetically stable by 7.64 kcal/mol than the forcefully optimized structure (Figure 10). Further, the geometry of the condensed product (peryald·MA) within the **CB2** cleft is successfully optimized and it is found that the product is ejecting out of the cleft. Figure S35 displays the optimized geometry of the peryald·MA within **CB2**, while the coordinates of optimized geometries are provided in supporting information.

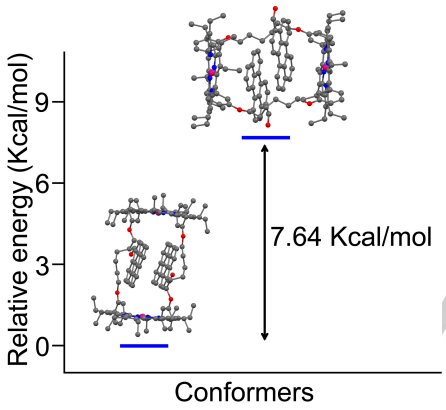

Figure 10. Relative energies of the optimized molecular structure of two differently oriented **CB2**·(peryald)$_2$.

Conclusion

In summary, we have synthesized three cyclic bisporphyrins varying chain lengths (and hence cavity size) that can preferentially encapsulate/coordinate various polycyclic aromatic aldehydes and thereby influence the reactivity in a controlled way. Different stacking arrangements are observed within the bisporphyrin cavity based on the host-guest size compatibility, which is substantiated by using UV-vis, ^{1}H NMR, and X-ray crystal structure determination. The preferential and efficient binding of the cyclic bisporphyrin hosts towards aromatic aldehyde as guest has been successfully utilized to catalyze the Knoevenagel condensation of a series of aromatic aldehydes with Meldrum's acid/1,3-dimethylbarbituric acid in aqueous THF medium. It is found that the condensation reactions are quite selective towards the polycyclic aromatic aldehydes here. Upon increasing the chain length and thereby cavity, the yield of the condensed product also increases. Thus, we have utilized here tunable bisporphyrinic container molecules to manifest a trademark feature of enzymatic catalysis. Moreover, such flexible molecular containers can be useful in developing artificial molecular devices and molecular machines. Efforts toward developing of these areas are currently under investigation.

Experimental Section

Materials: All the reagents and solvents are purchased from commercial sources and purified by standard procedures before use. 3-formylperylene was synthesized according to a reported procedure.[18] Zn(II) cyclic bisporphyrin hosts, **CB1** and **CB2** have been prepared using the procedures reported earlier.[13c,d] **CB3** have been synthesized according to the synthetic strategy displayed in Scheme S1. 5, 15-bis (3′-hydroxyphenyl)-octaethylporphyrin, **A** was synthesized according to a reported procedure.[13b] The other synthetic steps and the preparation host-guest complexes, reported in the present work, are described below.

Preparation of 5,l5-bis(3′-(1-bromooctanyloxy) phenyl)-octaethylporphyrin, B: Into a 100 mL round-bottom flask equipped with a magnetic stir bar and a water-cooled reflux condenser were combined with **A** (100 mg, 0.14 mmol), K_2CO_3 (100 mg, 0.72 mmol), 18-crown-6 (20 mg, 0.075 mmol), dry acetone (50 mL), and 1,8-dibromooctane (3.0 g, 11.02 mmol) and the resulting mixture was refluxed under N_2 atmosphere for 12 h. The reaction mixture was then cooled to room temperature, filtered, and further washed with 50 mL acetone. The combined solution was evaporated to dryness and it was further purified by silica gel column chromatography (hexane/CH_2Cl_2 2:1 v/v) to yield the desired product as a red solid. Yield: 141 mg (92%). ^{1}H NMR ($CDCl_3$, 298 K): 10.29 (*s*, 2H; *meso-H*), 7.92 (*d*, 2H; Ar-*H*), 7.86 (*s*, 2H; Ar-*H*), 7.62 (*t*, 2H; Ar-*H*), 7.40 (*d*, 2H; Ar-*H*), 4.19 (*t*, 4H; -OCH_2), 3.56 (*t*, 4H; -CH_2Br), 3.43 (*m*, 8H; -CH_2CH$_3$), 3.28 (*m*, 8H; -CH_2CH$_3$), 2.92 (*m*, 12H; -OCH$_2$C$_6$H$_{12}$CH$_2$Br), 1.96 (*m*, 12H; -OCH$_2$C$_6$H$_{12}$CH$_2$Br), 1.82 (*t*, 12H; -CH$_2$CH$_3$), 1.35 (*t*, 12H; -CH$_2$CH$_3$), -2.18 (*br*, 2H, -N*H*); UV-vis (CH_2Cl_2) [λ_{max}, nm (ε, M^{-1} cm^{-1})]: 411 (5.0 x 10^5), 509 (1.6 x 10^4), 541 (1.2 x 10^4), 577 (5.3 x 10^3), 631(3.0 x 10^3); ESI-MS: *m*/*z* 1100.51[M]$^+$.

Preparation of free base cyclic bisporphyrin, C: To a magnetically stirred DMF suspension (150 mL) of K_2CO_3 (600 mg, 4.32 mmol) in a 250 mL round-bottom flask was added dropwise a DMF solution (25 mL) of **A** (200 mg, 0.278 mmol) and **B** (306 mg, 0.278 mmol) over a period of 12 h. After the addition was completed, the reaction mixture was allowed to stir for an additional 60 h. Then the reaction mixture was poured into toluene (300 mL), washed with water (2×200 mL), dried over Na_2SO_4, and evaporated to dryness. The cyclic dimer was purified by silica gel column chromatography (hexane/CH_2Cl_2 1:1 v/v), where the second band was collected and evaporated to dryness to afford **C** as reddish solid. Yield: 110 mg (24%).^{1}H NMR ($CDCl_3$, 298 K): 10.14 (*s*, 4H; *meso-H*), 7.78-7.28 (*m*, 16H; Ar-*H*), 3.98 (*m*, 20H; -OCH_2, -CH_2CH$_3$), 3.24 (*m*, 12H; -CH_2CH$_3$), 2.72 (*m*, 16H; -OCH$_2$C$_6$H$_{12}$CH$_2$Br, -CH_2CH$_3$), 2.12-0.92 (*m*, 64H; -CH_2CH$_3$, -OCH$_2$C$_6$H$_{12}$CH$_2$Br, -CH$_2$CH_3), -2.22 (*br*, 4H, -N*H*); UV-vis (CH_2Cl_2) [λ_{max}, nm (ε, M^{-1} cm^{-1})]: 412 (5.0 x 10^5), 509 (4.5 x 10^4), 540 (3.1 x 10^4), 578 (1.1 x 10^4), 631(6.5 x 10^3); ESI-MS: *m*/*z* 1659.11 [M+H]$^+$.

Preparation of Zn(II) cyclic bisporphyrin, CB3: To a magnetically stirred solution of **C** (100 mg, 0.06 mmol) in chloroform (50 mL) in a 250 mL round-bottom flask was added a solution of $Zn(OAc)_2$ (100 mg, 0.54 mmol) in methanol (10 mL). The resulting mixture was allowed to stir at room temperature for 5-6 h. The reaction mixture was then evaporated and the residue was purified by silica gel column chromatography (hexanes/CH_2Cl_2 1:1 v/v) to yield the desired product **CB3** as a bright red solid. Yield: 100 mg (93%). ^{1}H NMR ($CDCl_3$, 298 K): 10.05 (*s*, 4H; *meso-H*), 7.84-7.30 (*m*, 16H; Ar-*H*), 4.02 (*m*, 20H; -OCH_2, -CH_2CH$_3$), 3.30 (*m*, 12H; -CH_2CH$_3$), 2.80 (*m*, 16H; -OCH$_2$C$_6$H$_{12}$CH$_2$Br, -CH_2CH$_3$), 1.87-0.88 (*m*, 64H; -CH_2CH$_3$, -OCH$_2$C$_6$H$_{12}$CH$_2$Br,-CH$_2$CH_3); UV-vis (CH_2Cl_2) [λ_{max}, nm (ε, M^{-1} cm^{-1})]: 410 (6.7 x 10^5), 540 (4.7 x 10^4), 575 (3.0 x 10^4); ESI-MS: *m*/*z* 1785.90 [M+H]$^+$.

All the host-guest complexes reported in the present work were prepared using the general procedure; details for one representative case are described below.

Preparation of CB1•peryald: To a solution of **CB1** (20 mg, 0.012 mmol) in 50 mL dichloromethane, peryald (30 mg, 0.107 mmol) was added and stirred at room temperature for 15 minutes. The resulting solution was then evaporated to complete dryness. The solid thus obtained was dissolved in a minimum volume of dichloromethane and carefully layered with acetonitrile which was then kept for slow diffusion in air. On standing for 6-7 days, dark red crystalline solid of the host-guest complex was formed in excellent yields which was then collected and dried in vacuum.

Yield: 17 mg (75%). ^{1}H NMR ($CDCl_3$, 298 K): 9.99 (*s*, 4H; *meso-H*), 9.88 (*s*, 1H; *CH*O), 8.78 (*d*, 1H; peryald-*H*), 7.85-7.16 (*m*, 26H; Ar-*H*, peryald-*H*), 4.10-3.74 (*m*, 16H; $OCH_2C_2H_4CH_2O$, $-CH_2CH_3$), 2.72-2.60 (*m*, 32H; $-OCH_2C_2H_4CH_2O$, $-CH_2CH_3$), 1.74 (*t*, 24H; $-CH_2CH_3$), 1.09 (*t*, 24H; $-CH_2CH_3$); UV-vis (CH_2Cl_2): [λ_{max}, nm (ε, $M^{-1}cm^{-1}$)]: 410 (3.5 x 10^5), 541 (1.8 x 10^4), 575 (6.2 x 10^3); ESI-MS: *m*/*z* 1953.86 $[M+H]^+$.

Preparation of CB2•(peryald)$_2$: Yield: 21 mg (78%). ^{1}H NMR ($CDCl_3$, 298 K): 10.01 (*s*, 4H; *meso-H*), 9.67 (*s*, 2H; *CH*O), 8.52 (*d*, 2H; peryald-*H*), 7.86-6.84 (*m*, 36H; Ar-*H*, peryald-*H*), 3.89-3.53 (*m*, 40H; $OCH_2C_4H_8CH_2O$, $-CH_2CH_3$), 2.68 (*m*, 16H; $-OCH_2C_4H_8CH_2O$), 1.75 (*t*, 24H; $-CH_2CH_3$), 1.07 (*t*, 24H; $-CH_2CH_3$); UV-vis (CH_2Cl_2) [λ_{max}, nm (ε, $M^{-1}cm^{-1}$)]: 411 (2.8 x 10^5), 540 (1.2 x 10^4), 575 (3.8 x 10^3); ESI-MS: *m*/*z* 1144.31 $[M+2H]^{2+}$.

Preparation of CB3•(peryald)$_2$: Yield: 18 mg (70%). ^{1}H NMR ($CDCl_3$, 298 K): 10.05 (*s*, 4H; *meso-H*), 9.82 (*br*, 2H; *CH*O), 8.77 (*br*, 2H; peryald-*H*), 7.83-7.18 (*m*, 36H; Ar-*H*, peryald-*H*), 4.03-3.87 (*m*, 20H; $OCH_2C_6H_{12}CH_2O$, $-CH_2CH_3$), 2.81-2.70 (*m*, 36H; $-OCH_2C_6H_{12}CH_2O$, $-CH_2CH_3$), 1.87-1.68 (*m*, 32H; $-CH_2CH_3$, $-CH_2CH_3$), 1.12 (*t*, 24H; $-CH_2CH_3$); UV-vis (CH_2Cl_2) [λ_{max}, nm (ε, M^{-1} cm^{-1})]: 412 (4.8 x 10^5), 540 (2.6 x 10^4), 575 (6.0 x 10^3); ESI-MS: *m*/*z* 2344.15 $[M+H]^+$.

Instrumentation: UV-visible spectra were recorded on a Perkin Elmer UV-Vis-NIR spectrometer. ^{1}H and ^{13}C NMR spectra were recorded on a JEOL 500 MHz instrument. The residual ^{1}H resonances of the solvents were used as a secondary reference. ESI-MS spectra were recorded on a Waters Micromass Quattro Micro triple quadropole mass spectrometer. Infrared (IR) spectra were recorded in the range of 4000–400 cm^{-1} with a Vertex 70 Bruker spectrophotometer on KBr pellets.

X-ray Structure Solution and Refinement: Crystals were coated with light hydrocarbon oil and mounted in the 100 K dinitrogen stream of a Bruker SMART APEX CCD diffractometer equipped with CRYO industries low temperature apparatus and intensity data were collected using graphite-monochromated Mo Ka radiation (λ=0.71073Å). The data integration and reduction were processed with SAINT software.[19] An absorption correction was applied.[20] Structures were solved by the direct method using SHELXS-97 and were refined on F^2 by full-matrix least-squares technique using the SHELXL-2014 program package.[21] Non-hydrogen atoms were refined anisotropically. In the refinement, the hydrogen atoms were included in geometrically calculated positions and were refined according to the "riding model".

CCDC 1531241 [**CB3•**(peryald)$_2$], 1531242 [**CB2•**(peryald)$_2$], 1531243 (**CB1•**Me-napald), 1531244 [**CB2•**(antald)$_2$], and 1531245 [**CB3•**(pyald)$_2$] contain the supplementary crystallographic data for this paper. These data are provided free of charge by The Cambridge Crystallographic Data Centre.

Computational details: DFT calculations have been carried out by using a B3LYP hybrid functional and the *Gaussian 03*, revision B.04, package.[17] The method used was Becke's three-parameter hybrid-exchange functional,[22] the non-local correlation provided by the Lee, Yang, and Parr expression, and the Vosko, Wilk, and Nuair 1980 correlation functional (III) for local correction.[23] The basis set was 6–31G** for C, N, O, and H atoms and LANL2DZ for Zn atom. Full geometry optimizations were done in which all the coordinates were taken from the single-crystal X-ray structure of the molecules. The optimized geometry was confirmed to be the potential energy minima by vibrational frequency calculations at the same level of theory as no imaginary frequencies were found. The orbital surfaces were visualized by *Chemcraft* software program. The molecular structures of all the complexes were also generated and prepared graphically with this software. The DFT optimized structures of **CB1•**peryald and **CB1•**pyald are displayed in Figures 9A and S34, respectively, and the computed bond distances and angles of **CB1•**peryald and **CB1•**pyald are shown in Tables S3.

Supporting information available: Synthetic scheme (Scheme S1), UV-vis spectral changes of **CB** with guest ligands (Figures S1, S2), experimental and simulated ESI-MS spectra of **CB1•**peryald, **CB2•**(peryald)$_2$ and **CB3•**(peryald)$_2$ (Figures S3, S4), molecular packing diagrams (Figures S5–S10), crystal data and data collection parameters (Table S1), ^{1}H NMR spectra (Figures S11, S12), association constant determinations (Figures S13–S15), typical procedure for the Knoevenagel condensation, ^{1}H NMR spectra of the condensed products (Figures S17–S32), tables of yields of the products (Table S2, S3), optimized geometries of **CB1•**pyald and peryald•MA within **CB2** (Figures S34, S35), atom numbering schemes (Figure S36), computed bond distances and angles (Table S4), cartesian coordinates of the optimized geometry.

Acknowledgements

We are thankful to Science and Engineering Research Board (SERB), India for financial support and PM thanks IIT Kanpur, for fellowship.

[1] a) C. J. Brown, F. D. Toste, R. G. Bergman, K. N. Raymond, *Chem. Rev*. **2015**, *115*, 3012-3035; b) P. Ballester, M. Fujita, J. Rebek Jr., *Chem. Soc. Rev*. **2015**, *44*, 392-393; c) D. S. Kim, J. L. Sessler, *Chem. Soc. Rev*. **2015**, *44*, 532-546; d) J. H. Jordan, B. C. Gibb, *Chem. Soc. Rev*. **2015**, *44*, 547-585.

[2] a) A. Harada, R. Kobayashi, Y. Takashima, A. Hashidzume, H. Yamaguchi, *Nat. Chem.* **2011**, *3*, 34-37; b) D. Fiedler, D. H. Leung, R. G. Bergman, K. N. Raymond, *Acc. Chem. Res.* **2005**, *38*, 351-360; c) F. Hof, S. L. Craig, C. Nuckolls, J. Rebek Jr., *Angew. Chem. Int. Ed*. **2002**, *41*, 1488-1508.

[3] a) V. Ramamurthy, J. Sivaguru, *Chem. Rev*. **2016**, *116*, 9914-9993; b) K. I. Assaf, W. M. Nau, *Chem. Soc. Rev*. **2015**, *44*, 394-418; c) S. Zarra, D. M. Wood, D. A. Roberts, J. R. Nitschke, *Chem. Soc. Rev.* **2015**, *44*, 419-432; d) S. H. A. M. Leenders, R. Gramage-Doria, B. de Bruin, J. N. H. Reek, *Chem. Soc. Rev*. **2015**, *44*, 433-448; e) M. D. Pluth, R. G. Bergman, K. N. Raymond, *Science* **2007**, *316*, 85-88.

[4] a) P. A. Gale, C. C. Tong, C. J. E. Haynes, O. Adeosun, D. E. Gross, E. Karnas, E. M. Sedenberg, R. Quesada, J. L. Sessler, *J. Am. Chem. Soc*. **2010**, *132*, 3240-3241; b) R. Cui, Q. Li, D. E. Gross, X. Meng, B. Li, M. Marquez, R. Yang, J. L. Sessler, Y. Shao, *J. Am. Chem. Soc*. **2008**, *130*, 14364-14365.

[5] a) T. Murase, Y. Nishijima, M. Fujita, *J. Am. Chem. Soc.* **2012**, *134*, 162-164; b) J. M. Wiester, P. A. Ulmann, C. A. Mirkin, *Angew. Chem. Int. Ed.* **2011**, *50*, 114-137; c) M. Yoshizawa, J. K. Klosterman, M. Fujita, *Angew. Chem. Int. Ed*. **2009**, *48*, 3418-3438.

[6] a) H. Furukawa, K. E. Cordova, M. O'Keeffe, O. M. Yaghi, *Science* **2013**, *341*, 1230444; b) B. Mondal, K. Acharyya, P. Howlader, P. S. Mukherjee, *J. Am. Chem. Soc.* **2016**, *138*, 1709-1716; c) B. Kang, J. W. Kurutz, K. T. Youm, R. K. Totten, J. T. Hupp, S. T. Nguyen, *Chem. Sci.* **2012**, *3*, 1938-1944; d) S. Dawn, M. B. Dewal, D. Sobransingh, M. C. Paderes, A. C. Wibowo, M. D. Smith, J. A. Krause, P. J. Pellechia, L. S. Shimizu, *J. Am. Chem. Soc*. **2011**, *133*, 7025–7032; e) Y. Nishioka, T. Yamaguchi, M. Yoshizawa, M. Fujita, *J. Am. Chem. Soc*. **2007**, *129*, 7000-7001.

[7] a) D. M. Kaphan, M. D. Levin, R. G. Bergman, K. N. Raymond, F. D. Toste, *Science* **2015**, *350*, 1235-1238; b) J. Meeuwissen, J. N. H. Reek, *Nat. Chem*. **2010**, *2*, 615-621; c) N. J. Turro, *Proc. Natl. Acad. Sci. USA* **2005**, *102*, 10766-10770; d) D. M. Vriezema, A. M. Comellas, J. A. A. W. Elemans, J. J. L. M. Cornelissen, A. E. Rowan, R. J. M. Nolte, *Chem. Rev*. **2005**, *105*, 1445-1490; e) A. M. Klibanov, *Nature* **2001**, *409*, 241-246.

[8] a) D. Wrobel, A. Graja, *Coord. Chem. Rev*. **2011**, *255*, 2555-2577; b) J. Rosenthal, D. G. Nocera, *Acc. Chem. Res*. **2007**, *40*, 543-553; c) M. Tanaka, K. Ohkubo, C. P. Gros, R. Guilard, S. Fukuzumi, *J. Am. Chem. Soc.* **2006**, *128*, 14625–14633; d) P. D. W. Boyd, C. A. Reed, *Acc. Chem. Res*. **2005**, *38*, 235-242; e) K. Lang, J. Mosinger, D. M. Wagnerova, *Coord. Chem. Rev*. **2004**, *248*, 321-350.

[9] a) P. Mondal, S. P. Rath, *Chem. Eur. J.* **2016**, *22*, 5607-5619; b) P. Mondal, S. P. Rath, *Isr. J. Chem*. **2016,** *56*, 144-155; c) P. Mondal, S. P. Rath, *Eur. J. Inorg. Chem*. **2015**, 4956-4964; d) P. Mondal, A.

Chaudhary, S. P. Rath, *Dalton Trans*. **2013**, *42*, 12381-12394; e) A. Chaudhary, S. P. Rath, *Chem. Eur. J*. **2012**, *18*, 7404-7417; f) A. Chaudhary, S. P. Rath, *Chem. Eur. J*. **2011**, *17*, 11478-11487. g) S. A. Ikbal, A. Dhamija, S. Brahma, S. P. Rath, *J. Org. Chem*. **2016**, *81*, 5440-5449; h) S. A. Ikbal, S. Brahma, S. P. Rath, *Chem. Commun.* **2015**, *51*, 895-898.

[10] a) T. Guchhait, S. Sasmal, F. S. T. Khan, S. P. Rath, *Coord. Chem. Rev*. **2017**, *337*, 112-144; b) F. S. T. Khan, T. Guchhait, S. Sasmal, S. P. Rath, *Dalton Trans.* **2017**, *46*, 1012-1037; c) F. S. T. Khan, A. K. Pandey, S. P. Rath, *Chem. Eur. J.* **2016**, *22*, 16124-16137; d) D. Sil, A. Kumar, S. P. Rath, *Chem. Eur. J.* **2016**, *22*, 11214-11223; e) D. Sil, S. P. Rath, *Dalton Trans*. **2015**, *44*, 16195-16211; f) S. K. Ghosh, S. Bhowmik, D. Sil, S. P. Rath, *Chem. Eur. J*. **2013**, *19*, 17846-17859; g) S. Bhowmik, S. Dey, D. Sahoo, S. P. Rath, *Chem. Eur. J*. **2013**, *19*, 13732-13744; h) S. Bhowmik, S. K. Ghosh, S. P. Rath, *Chem. Commun*. **2011**, *47*, 4790-4792; i) S. K. Ghosh, S. P. Rath, *J. Am. Chem*. *Soc*. **2010**, *132*, 17983-17985.

[11] a) I. Beletskaya, V. S. Tyurin, A. Y. Tsivadze, R. Guilard, C. Stern, *Chem*. *Rev*. **2009**, *109*, 1659-1713; b) K. Tashiro, T. Aida, *Chem. Soc. Rev*. **2007**, *36*, 189-197; c) P. D. Harvey, C. Stern, C. P. Gros, R. Guilard, *Coord. Chem. Rev*. **2007**, *251*, 401-428.

[12] a) M. Nakash, J. K. M. Sanders, *J. Org. Chem*. **2000**, *65*, 7266-7271; b) K. Tashiro, T. Aida, J.-Y. Zheng, K. Kinbara, K. Saigo, S. Sakamoto, K. Yamaguchi, *J. Am. Chem. Soc*. **1999**, *121*, 9477-9478.

[13] a) L. P. Hernandez-Eguía, E. C. Escudero-Adan, J. R. Pinzon, L. Echegoyen, P. Ballester, *J. Org. Chem*. **2011**, *76*, 3258-3265; b) Y. Shoji, K. Tashiro, T. Aida, *J. Am. Chem. Soc*. **2010**, *132*, 5928-5929; c) A. Ouchi, K. Tashiro, K. Yamaguchi, T. Tsuchiya, T. Akasaka, T. Aida, *Angew. Chem. Int. Ed*. **2006**, *45*, 3542-3546; d) J.-Y. Zheng, K. Tashiro, Y. Hirabayashi, K. Kinbara, K. Saigo, T. Aida, S. Sakamoto, K. Yamaguchi, *Angew. Chem. Int. Ed*. **2001**, *40*, 1857-1861.

[14] a) Z.- A. Qiao, P. Zhang, S.-H. Chai, M. Chi, G. M. Veith, N. C. Gallego, M. Kidder, S. Dai, *J. Am. Chem*. *Soc*. **2014**, *136*, 11260-11263; b) Q. Han, C. He, M. Zhao, B. Qi, J. Niu, C. Duan, *J. Am. Chem. Soc*. **2013**, *135*, 10186-10189; c) N. Mizuno, S. Uchida, K. Kamata, R. Ishimoto, S. Nojima, K. Yonehara, Y. Sumida, *Angew. Chem. Int. Ed*. **2010**, *49*, 9972-9976; d) S. Horike, M. Dincă, K. Tamaki, J. R. Long, *J. Am. Chem. Soc*. **2008**, *130*, 5854-5855.

[15] a) M. Otte, *ACS Catal*. **2016**, *6*, 6491-6510; b) Y. Qiao, L. Zhang, J. Li, W. Lin, Z. Wang, *Angew. Chem. Int. Ed*. **2016**, *55*, 1-6; c) C. G. Oliveri, N. C. Gianneschi, S. T. Nguyen, C. A. Mirkin, C. L. Stern, Z. Wawrzak, M. Pink, *J. Am. Chem. Soc*. **2006**, *128*, 16286-16296.

[16] a) http://www.hyperquad.co.uk/HypSpec.htm; b) P. Gans, A. Sabatini, A. Vacca, *Talanta* **1996**, *43*, 1739-1753.

[17] M. J. T. Frisch, G. W. Trucks, H. B. Schlegel, G. E. Scuseria, M. A. C. Robb, J. R. Cheeseman, G. Scalmani, V. Barone, G. A. N. B. Mennucci, H. Petersson, M. Caricato, X. Li, H. Hratchian, A. F. Izmaylov, J. Bloino, G. Zheng, J. L. Sonnenberg, M. Hada, M. Ehara, K. Toyota, R. Fukuda, J. Hasegawa, M. Ishida, Y. K. T. Nakajima, O. Honda, H. Nakai, T. Vreven, J. A. Montgomery, J. E. O. Peralta Jr., F. Oligaro, M. Bearpark, J. J. Heyd, E. Brothers, V. N. Kudin, K. K.N. R. Staroverov, J. Normand, K. Raghavachari, A. B. Rendell, S. S. Iyengar, J. Tomasi, M. Cossi, J. M. Rega, M. Millam, J. E. Knox, J. B. Cross, V. Bakken, C. J. Adamo, J. Gomperts, R. E. Stratmann, O. Yazyev, A. J. Austin, R. Cammi, J. W. Pomelli, J. W. Ochterski, R. L. Martin, K. Z. Morokuma, V. G. Zarkrzewski, G. A. Voth, P. Salvador, J. J. D. Dannenberg, S. Dapprich, A. D. Daniels, Ö. Farkas, J. B. Foresman, J. V. Ortiz, J. Cioslowski, D. J. Fox Gaussian 09, Revision B.01, Gaussian, Inc., Wallingford, CT, **2010**.

[18] K. Kodama, A. Kobayashi, T. Hirose, *Tetrahedron Lett.* **2013**, *54*, 5514-5517.

[19] *SAINT+*, version 6.02, Bruker AXS, Madison, WI, **1999**.

[20] G. M. Sheldrick, *SADABS 2.0*, 2000.

[21] G. M. Sheldrick, *SHELXL-2014*: *Program for Crystal Structure Refinement*, University of Gottingen, Gottingen, **2014**.

[22] A. D. Becke, *J. Chem. Phys*. **1993**, *98*, 5648-5652.

[23] C. Lee, W. Yang, R. G. Parr, *Phys. Rev. B.* **1988**, *37*, 785-789.

10.1002/chem.201700577

WILEY-VCH

Table of Contents

FULL PAPER

Three cyclic zinc(II) bisporphyrins (**CB**) with flexible linkers are employed as artificial molecular containers. Interestingly, the arrangements of the guests and the reactivity inside the containers are significantly influenced by the cavity size of the cyclic containers.

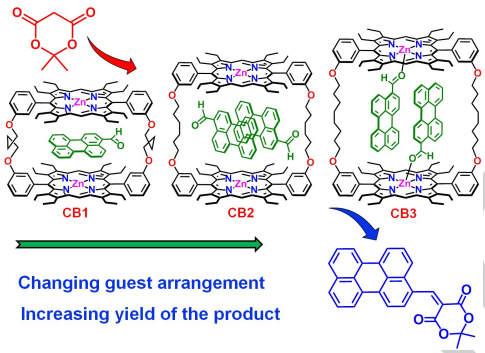

*Pritam Mondal, Sabyasachi Sarkar and Sankar Prasad Rath**

Page No. – Page No.

Cyclic Bisporphyrin Based Flexible Molecular Containers: Controlling Guest Arrangements and Supramolecular Catalysis by Tuning Cavity Size